ChemComm

COMMUNICATION

A tale of two forces: simultaneous chemical and acoustic propulsion of bimetallic micromotors†

Cite this: *Chem. Commun.*, 2015, **51**, 1020

Received 16th November 2014,
Accepted 26th November 2014

DOI: 10.1039/c4cc09149c

www.rsc.org/chemcomm

Wei Wang,[a] Wentao Duan,[b] Zexin Zhang,[c] Mei Sun,[a] Ayusman Sen[b] and Thomas E. Mallouk*[bde]

Bimetallic gold–ruthenium microrods are propelled in opposite directions in water by ultrasound and by catalytic decomposition of hydrogen peroxide. This property was used to effect reversible swarming, to stall and reverse autonomous axial propulsion, and to study the chemically powered movement of acoustically levitated microrods.

Synthetic nano- and microscale motors locally convert chemical[1–4] or other forms of energy (magnetic,[5–9] electrical,[10–12] photochemical,[13,14] acoustic,[15–23] thermal[24,25]) to mechanical movement. These microscopic motors, which move autonomously in fluids, are of interest for a growing number of applications that include chemical analysis[26–29] and separations,[30–36] repair of cracks in materials,[37] pumping of fluids in microchannels,[38–40] and prevention of membrane fouling.[41] Autonomously powered micro- and nanoparticles are also of fundamental interest as components of active matter.[42,43] They exhibit collective behavior, such as swarming and predator–prey interactions, that is mimetic of living organisms.[44–51] Such behavior is unique to powered systems, which form dynamic steady states that exist far from equilibrium. Understanding the forces that give rise to motor–motor interactions is important for rationalizing and predicting collective motor behavior, and also for developing new applications.[52–54]

To date most studies of micromotors have involved chemical propulsion. Hydrogen peroxide decomposition and photochemical reactions at the surface of catalytic motors generate chemical concentration gradients. These gradients move particles by electrophoresis and diffusiophoresis, and they can also pump fluids by means of electroosmosis and density gradients. Catalytically generated gradients and viscous forces can extend over tens or even hundreds of microns, leading to the very rich collective behavior of chemically powered motors. Recently, we and others have discovered that micron-size bimetallic rods, which were originally developed as catalytic motors, can also be propelled at speeds up to 200 μm s^{-1} by acoustic energy.[15–23] This propulsion mechanism relies on the shape asymmetry of the particles, rather than its chemical asymmetry. Acoustic propulsion is biocompatible, requiring no toxic fuels, but it does not generate the chemical gradients that are responsible for the interesting motor–motor interactions that are observed in other systems.

So far, relatively few studies have explored the dynamic interplay between multiple motor propulsion mechanisms. Wang and coworkers examined micromotors driven by magnetic and chemical forces, and demonstrated switching between the two modes of propulsion.[55] Here we report the movement and collective behavior of bimetallic micro-rods that are propelled in opposite directions by chemical and acoustic forces. By controlling the power of the acoustic field we find that we can stall or reverse the direction of movement. By observing forward and backward motion of the same particles, we separate the effects of axial propulsion and acoustic radiation force on particle movement. In addition, we are able to drive a fast and reversible transition between aggregated and free-moving states in response to a change of external stimuli (*i.e.*, the acoustic power), a functionality that may be useful in analytical applications.

Au–Ru microrods (~3 μm long and ~300 nm in diameter) were grown by template-assisted electrodeposition as described previously (see ESI† for Experimental details).[16,18,19] These microrods were suspended in 10% H_2O_2, and the suspension was added to a capillary cell with an ultrasonic transducer at the bottom that generated a vertical acoustic standing wave at ~3.7 MHz. Previous experiments in similar cell geometry have shown that metallic microrods are levitated to the midpoint plane of the cell, where the acoustic standing wave has a node.[16] In this plane Au–Ru rods

[a] *School of Material Science and Engineering, Harbin Institute of Technology, Shenzhen Graduate School, Shenzhen, 518055, China*
[b] *Department of Chemistry, The Pennsylvania State University, University Park, PA, 16802, USA. E-mail: tem5@psu.edu*
[c] *Center for Soft Condensed Matter Physics and Interdisciplinary Research, Soochow University, Suzhou, 215006, China*
[d] *Department of Biochemistry and Molecular Biology, The Pennsylvania State University, University Park, PA, USA*
[e] *Department of Physics, The Pennsylvania State University, University Park, PA, USA*

† Electronic supplementary information (ESI) available. See DOI: 10.1039/c4cc09149c

are propelled along their long axis by ultrasound and exhibit fast (up to ~200 μm s^{-1}) directional motion with the Ru end leading. In addition to simple axial propulsion, which has recently been shown by Nadal and Lauga to arise from the axially asymmetric shape of the rods,[15] several other behaviors are observed. These include tight circular orbits of rods in some regions of the levitation plane, the formation of ring structures and chaining of rapidly spinning rods. These patterns of movement appear to be controlled by acoustic radiation forces within the levitation plane, although it has been proposed that other shape asymmetry effects, such as curvature or helicity of the rods, can contribute to spinning or orbital movement.[16] In addition, Au–Ru microrods are subject to a catalytically generated axial force in H_2O_2 solutions. Under chemical power, Au–Ru microrods move with their Au end forward, the opposite of the direction of acoustic propulsion. The catalytic decomposition of H_2O_2 additionally generates a proton gradient in the solution around microrods, resulting in a dipolar electric field through which chemically powered microrods interact.

When the ultrasonic power is switched on, rods at the bottom of the cell are rapidly (~1 s) levitated to the midplane. The rods settle slowly (several seconds) with the power off, so it is possible to observe their movement in the levitation plane with and without ultrasonic excitation. In ultrasound the Au–Ru rods move with their Ru ends leading at an average speed of 63 ± 7 μm s^{-1} (Fig. 1 and Videos S1 and S2, see ESI†). We define this direction as "forward" movement. Under acoustic power, the movements of the rods appear independent of each other and there is little re-orientation during trajectories of tens of microns. In contrast, with the ultrasound turned off, the Au–Ru rods move with their Au ends forward ("backward" motion) at 33 ± 6 μm s^{-1}. This chemically propelled movement was autonomous, but less directional, presumably because Brownian re-orientation has a greater effect at slower axial speeds. By gradually stepping down the ultrasonic power we could lower the acoustic propulsion force, enabling us to stall the axial movement of the rods and reverse their direction under chemical propulsion. This is illustrated in Fig. S2 (ESI†).

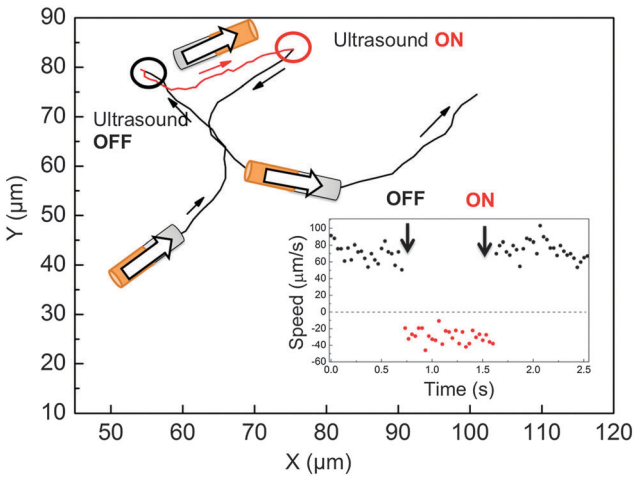

Fig. 1 Trajectory and speed changes (inset) of a levitated Au–Ru micromotor as the ultrasound power is switched on and off. Cartoons of Au–Ru rods are added to illustrate the direction of movement (not to scale). The movements of the motor in acoustic (forward) and chemical (backward) propulsion are colored in black and red respectively, with the forward speed defined as positive in the inset.

Interestingly, by comparing the chemical propulsion speeds of the same batch of Au–Ru rods moving in the central nodal plane (33 ± 6 μm s^{-1}) with those moving at the bottom of the cell (20 ± 4 μm s^{-1}, Video S3, ESI†), both in the absence of ultrasound, we observed an increase in speed of ~40% simply by lifting the motors away from the floor of the cell. This increase in speed agrees well with our previous study,[56] in which we estimated that contact with the charged floor of the cell should lower motor speeds by ~50% due to catalytically induced electroosmotic flow.

Analysis of motor trajectories (Fig. 1) revealed very weak correlation between the speed and directionality of propulsion by ultrasound and chemical forces. In each case there was a distribution of speeds, but the motors that moved faster in ultrasound (corrected for the backward chemical propulsion) did not necessarily move fastest under chemical power only (see Table S1 in ESI†). This is not surprising considering that the forward and backward movements are driven by completely different mechanisms. Motors that tended to move along circular trajectories in ultrasound moved without any directional bias once the acoustic power was turned off. These motors quickly resumed their orbital trajectories once the acoustic power was re-applied. This suggests that the orbital movement is not a consequence of rod curvature or other shape effects, but rather arises from in-plane acoustic forces.

Acoustic forces within the levitation plane (and also at the bottom of the cell) can compress the microrods into roughly circular aggregates or spinning chains. These effects appear to arise from acoustic nodal structure and reflection of sound waves, which depend on the geometry of the transducer and the cell. Interestingly, chemical propulsion causes these aggregates and chains to "explode" when the acoustic power is turned off, as illustrated in Fig. 2 and 3 and Videos S4–S7 (ESI†).

At the cell bottom (when ultrasound does not form a standing wave), Au–Ru rods exhibited aggregation–dispersion transitions when the ultrasound was switched on and off (Fig. 2). When the acoustic power was on, the rods followed the distribution of the acoustic energy and condensed into large bands (2a) or small clusters (2c). The location, shape and sizes of these aggregates varied, presumably reflecting the inhomogeneous distribution of acoustic energy. Individual rods were arranged densely and in random orientations in these aggregates, but were dynamic and in constant motion. Over the course of several seconds, most of the rods condensed into these clusters with few "free" motors between them. When the sound was turned off, the clusters exploded through a combination of axial movement and Brownian re-orientation, which is characteristic of chemical propulsion. Within seconds, the aggregates disintegrated into a dispersion of individual free-moving microrods. This rapid transition (captured in Fig. 2 in snapshots from Videos S6 and S7, ESI†) between the aggregated state and free-moving motors indicates that the acoustic force that holds microrods together in an aggregate immediately disappears when the field is turned off. We also observed that some of the microrods remained in clusters even after the sound was turned off, and there were microrods that dynamically assembled into pairs and triplets with their neighbours when chemically propelled.

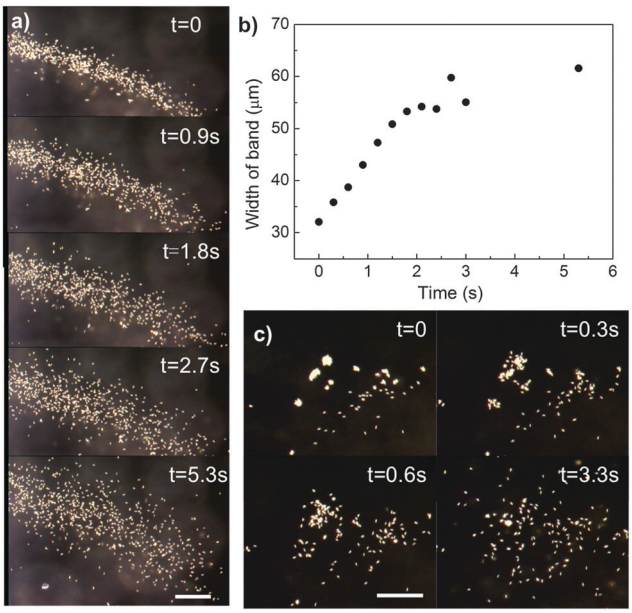

Fig. 2 Transition between aggregated and dispersed states of a group of Au–Ru microrods at the acoustic cell bottom. (a) Snapshots of the disintegration of a loose band of Au–Ru microrods at different times (ultrasound was turned off at t = 0); (b) the width of the band in (a) as a function of time; (c) snapshots of the disintegration of a tight cluster of Au–Ru microrods at different times (ultrasound was turned off at t = 0). Scale bar: 50 μm.

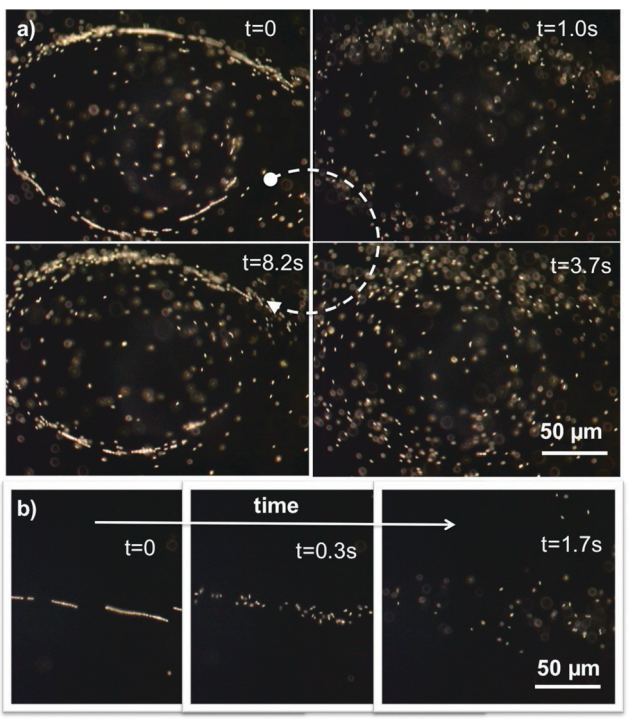

Fig. 3 Transition between aggregated and dispersed states of a group of Au–Ru microrods at the acoustic nodal plane. (a) Snapshots of the disintegration (sound off at t = 0) and reassembly (sound on at t = 3.7 s) of a ring structure made of Au–Ru microrods at different times; (b) snapshots of the disintegration (sound off at t = 0) of a Au–Ru microrod chain of one rod in width at different times. Scale bar: 50 μm.

These observations indicate attractive interactions among microrods that presumably originate from chemical gradients as demonstrated previously for pairs and triplets of chemically powered motors.[57]

By analyzing how the rods moved away from the clusters/bands when the ultrasound was turned off, we obtained additional information about the collective behavior of self-propelled microrods. First, we tracked the growth of the width of one particular band structure (Fig. 2a) formed by microrods at the cell bottom (see ESI† for details). The width of the band grew linearly with time at the beginning of the chemically driven explosion, but slowed down at longer times (Fig. 2b). Simple powered diffusion should result in a width that increases with $t^{1/2}$, which appears to be the limiting behavior at long times. The early time behavior may reflect attractive interactions between powered rods.[57] This is consistent with the observation (comparing Fig. 2a and c) that the density of rods in an aggregate affects the rate at which they disperse. Similar collective behavior has been observed with natural microorganisms such as bacteria at high population densities.[58,59]

At the central nodal plane (when ultrasound forms a standing wave), Au–Ru microrods could also be switched between states of organized assembly and random movement by switching ultrasound on and off (Fig. 3). This was particularly clear for ring aggregates that are formed by spinning chains of rods (Fig. 3a and Video S4, ESI†). Within these rings, individual microrods exhibited axially directed movement along the chain (in both clockwise and counter-clockwise directions), and fast spinning around the chain axis. These circulating and spinning behaviors have been noted previously,[16] and it has been determined that the rods spin at kilohertz frequency.[23] At low particle density, the most salient feature of these aggregates is the assembly of rods into a polar chain that is one rod in width (Fig. 3b and Video S5, ESI†). In the presence of H_2O_2, however, the microrods immediately reversed their directions and the rods in the chains were completely dispersed when the ultrasonic power was turned off.

The reversible compression of motors into dense aggregates illustrated in Fig. 2 and 3, as well as the stalling of movement by matching chemical and acoustic forces (Fig. 1), are of potential interest for analytical applications. Sheehan and Whitman have shown that biological analytes that are present at femtomolar concentrations can take very long times to collect by simple diffusion at ultramicroelectrodes.[60] Powered microrods can range very rapidly over sampling distances of hundreds of μm and can also catch and release "cargo" particles of various kinds.[61–63] This suggests possible schemes for delivery of analytes to sensor elements in microfluidic devices.

Bimetallic microrods that are propelled by hydrogen peroxide decomposition can be made to reverse directions under changing environmental cues (ultrasound). There are so far two other micromotor systems that can perform similar functions. Flexible magnetic rods can be propelled forward in rotating magnetic fields and backward by self-electrophoresis.[55] Magnetic microhelices can move forward or backward depending on which way the rotating magnetic field is applied.[7] The combined acoustic-chemical propulsion scheme demonstrated here combines two completely autonomous propulsion modes, and also enables the reversible

collection of motors into dense aggregates. Cycling between the on and off states of ultrasound causes the entire population of Au–Ru microrods to undergo fast transitions between aggregated states (or organized assembly) to freely-moving autonomous motors. Similar behavior may emerge in other dual propulsion systems, *e.g.*, shape-asymmetric motors that are chemically powered by bubble propulsion.[64] These behaviors can impart to micromotors useful functionality for applications, *e.g.*, in trace analysis and particle separations. These applications will be explored in future studies.

This work was supported by the National Science Foundation under MRSEC grant number DMR-0820404. WW and MS are grateful for the financial support from National Natural Science Foundation of China (Grant No. 11402069).

Notes and references

1 W. F. Paxton, K. C. Kistler, C. C. Olmeda, A. Sen, S. K. St Angelo, Y. Cao, T. E. Mallouk, P. E. Lammert and V. H. Crespi, *J. Am. Chem. Soc.*, 2004, **126**, 13424–13431.
2 M. Pumera, *Nanoscale*, 2010, **2**, 1643–1649.
3 S. Fournier-Bidoz, A. C. Arsenault, I. Manners and G. A. Ozin, *Chem. Commun.*, 2005, 441–443.
4 J. Gibbs and Y. Zhao, *Front. Mater. Sci.*, 2011, **5**, 25–39.
5 R. Dreyfus, J. Baudry, M. L. Roper, M. Fermigier, H. A. Stone and J. Bibette, *Nature*, 2005, **437**, 862–865.
6 L. Zhang, J. J. Abbott, L. Dong, K. E. Peyer, B. E. Kratochvil, H. Zhang, C. Bergeles and B. J. Nelson, *Nano Lett.*, 2009, **9**, 3663–3667.
7 S. Tottori, L. Zhang, F. Qiu, K. K. Krawczyk, A. Franco-Obregon and B. J. Nelson, *Adv. Mater.*, 2012, **24**, 811–816.
8 P. Fischer and A. Ghosh, *Nanoscale*, 2011, **3**, 557–563.
9 A. Ghosh and P. Fischer, *Nano Lett.*, 2009, **9**, 2243–2245.
10 S. T. Chang, V. N. Paunov, D. N. Petsev and O. D. Velev, *Nat. Mater.*, 2007, **6**, 235–240.
11 G. Loget and A. Kuhn, *J. Am. Chem. Soc.*, 2010, **132**, 15918–15919.
12 P. Calvo-Marzal, S. Sattayasamitsathit, S. Balasubramanian, J. R. Windmiller, C. Dao and J. Wang, *Chem. Commun.*, 2010, **46**, 1623–1624.
13 Y. Hong, M. Diaz, U. M. Córdova-Figueroa and A. Sen, *Adv. Funct. Mater.*, 2010, **20**, 1568–1576.
14 M. Liu, T. Zentgraf, Y. Liu, G. Bartal and X. Zhang, *Nat. Nanotechnol.*, 2010, **5**, 570–573.
15 F. Nadal and E. Lauga, *Phys. Fluids*, 2014, **26**, 082001.
16 W. Wang, L. A. Castro, M. Hoyos and T. E. Mallouk, *ACS Nano*, 2012, **6**, 6122–6132.
17 D. Kagan, M. J. Benchimol, J. C. Claussen, E. Chuluun-Erdene, S. Esener and J. Wang, *Angew. Chem., Int. Ed.*, 2012, **51**, 7519–7522.
18 W. Wang, S. Li, L. Mair, S. Ahmed, T. J. Huang and T. E. Mallouk, *Angew. Chem., Int. Ed.*, 2014, **53**, 3201–3204.
19 S. Ahmed, W. Wang, L. O. Mair, R. D. Fraleigh, S. Li, L. A. Castro, M. Hoyos, T. J. Huang and T. E. Mallouk, *Langmuir*, 2013, **29**, 16113–16118.
20 V. Garcia-Gradilla, J. Orozco, S. Sattayasamitsathit, F. Soto, F. Kuralay, A. Pourazary, A. Katzenberg, W. Gao, Y. F. Shen and J. Wang, *ACS Nano*, 2013, **7**, 9232–9240.
21 V. Garcia-Gradilla, S. Sattayasamitsathit, F. Soto, F. Kuralay, C. Yardımcı, D. Wiitala, M. Galarnyk and J. Wang, *Small*, 2014, **10**, 4154–4159.
22 S. Ahmed, D. T. Gentekos, C. A. Fink and T. E. Mallouk, *ACS Nano*, 2014, **8**, 11053–11060.
23 A. L. Balk, L. O. Mair, P. P. Mathai, P. N. Patrone, W. Wang, S. Ahmed, T. E. Mallouk, J. A. Liddle and S. M. Stavis, *ACS Nano*, 2014, **8**, 8300–8309.
24 H. R. Jiang, N. Yoshinaga and M. Sano, *Phys. Rev. Lett.*, 2010, **105**, 268302.
25 L. Baraban, R. Streubel, D. Makarov, L. Han, D. Karnaushenko, O. G. Schmidt and G. Cuniberti, *ACS Nano*, 2012, **7**, 1360–1367.
26 J. Wu, S. Balasubramanian, D. Kagan, K. M. Manesh, S. Campuzano and J. Wang, *Nat. Commun.*, 2010, **1**, 36.
27 J. Orozco, V. García-Gradilla, M. D'Agostino, W. Gao, A. Cortés and J. Wang, *ACS Nano*, 2012, **7**, 818–824.
28 D. Kagan, P. Calvo-Marzal, S. Balasubramanian, S. Sattayasamitsathit, K. M. Manesh, G. U. Flechsig and J. Wang, *J. Am. Chem. Soc.*, 2009, **131**, 12082–12083.
29 J. G. S. Moo, H. Wang, G. J. Zhao and M. Pumera, *Chem. – Eur. J.*, 2014, **20**, 4292–4296.
30 G. J. Zhao, H. Wang, S. Sanchez, O. G. Schmidt and M. Pumera, *Chem. Commun.*, 2013, **49**, 5147–5149.
31 M. Guix, J. Orozco, M. Garcia, W. Gao, S. Sattayasamitsathit, A. Merkoci, A. Escarpa and J. Wang, *ACS Nano*, 2012, **6**, 4445–4451.
32 S. Sanchez, A. A. Solovev, S. Schulze and O. G. Schmidt, *Chem. Commun.*, 2011, **47**, 698–700.
33 D. Kagan, S. Campuzano, S. Balasubramanian, F. Kuralay, G.-U. Flechsig and J. Wang, *Nano Lett.*, 2011, **11**, 2083–2087.
34 S. Balasubramanian, D. Kagan, C.-M. Jack Hu, S. Campuzano, M. J. Lobo-Castañon, N. Lim, D. Y. Kang, M. Zimmerman, L. Zhang and J. Wang, *Angew. Chem., Int. Ed.*, 2011, **50**, 4161–4164.
35 S. Campuzano, J. Orozco, D. Kagan, M. Guix, W. Gao, S. Sattayasamitsathit, J. C. Claussen, A. Merkoçi and J. Wang, *Nano Lett.*, 2011, **12**, 396–401.
36 K. K. Dey, S. Das, M. F. Poyton, S. Sengupta, P. J. Butler, P. S. Cremer and A. Sen, *ACS Nano*, DOI: 10.1021/nn504418u.
37 V. Yadav, J. D. Freedman, M. Grinstaff and A. Sen, *Angew. Chem., Int. Ed.*, 2013, **52**, 10997–11001.
38 S. Sengupta, M. M. Spiering, K. K. Dey, W. T. Duan, D. Patra, P. J. Butler, R. D. Astumian, S. J. Benkovic and A. Sen, *ACS Nano*, 2014, **8**, 2410–2418.
39 I.-K. Jun and H. Hess, *Adv. Mater.*, 2010, **22**, 4823–4825.
40 S. Sengupta, D. Patra, I. Ortiz-Rivera, A. Agrawal, S. Shklyaev, K. K. Dey, U. Cordova-Figueroa, T. E. Mallouk and A. Sen, *Nat. Chem.*, 2014, **6**, 415–422.
41 A. Kar, R. Guha, N. Dani, D. Velegol and M. Kumar, *Langmuir*, 2014, **30**, 793–799.
42 M. C. Marchetti, J. F. Joanny, S. Ramaswamy, T. B. Liverpool, J. Prost, M. Rao and R. A. Simha, *Rev. Mod. Phys.*, 2013, **85**, 1143.
43 X.-q. Shi and Y.-q. Ma, *Nat. Commun.*, 2013, **4**, 3013.
44 M. Ibele, T. E. Mallouk and A. Sen, *Angew. Chem., Int. Ed.*, 2009, **48**, 3308–3312.
45 J. G. Gibbs and Y. Zhao, *Small*, 2010, **6**, 1656–1662.
46 D. Kagan, S. Balasubramanian and J. Wang, *Angew. Chem., Int. Ed.*, 2011, **50**, 503–506.
47 A. A. Solovev, S. Sanchez and O. G. Schmidt, *Nanoscale*, 2013, **5**, 1284–1293.
48 W. Duan, R. Liu and A. Sen, *J. Am. Chem. Soc.*, 2013, **135**, 1280–1283.
49 M. E. Ibele, P. E. Lammert, V. H. Crespi and A. Sen, *ACS Nano*, 2010, **4**, 4845–4851.
50 J. Palacci, S. Sacanna, A. P. Steinberg, D. J. Pine and P. M. Chaikin, *Science*, 2013, **339**, 936–940.
51 I. Theurkauff, C. Cottin-Bizonne, J. Palacci, C. Ybert and L. Bocquet, *Phys. Rev. Lett.*, 2012, **108**, 268303.
52 S. J. Ebbens and J. R. Howse, *Soft Matter*, 2010, **6**, 726–738.
53 W. Wang, W. Duan, S. Ahmed, T. E. Mallouk and A. Sen, *Nano Today*, 2013, **8**, 531–534.
54 P. H. Colberg, S. Y. Reigh, B. Robertson and R. Kapral, *Acc. Chem. Res.*, DOI: 10.1021/ar5002582.
55 W. Gao, K. M. Manesh, J. Hua, S. Sattayasamitsathit and J. Wang, *Small*, 2011, **7**, 2047–2051.
56 W. Wang, T.-Y. Chiang, D. Velegol and T. E. Mallouk, *J. Am. Chem. Soc.*, 2013, **135**, 10557–10565.
57 W. Wang, W. Duan, A. Sen and T. E. Mallouk, *Proc. Natl. Acad. Sci. U. S. A.*, 2013, **110**, 17744–17749.
58 N. C. Darnton, L. Turner, S. Rojevsky and H. C. Berg, *Biophys. J.*, 2010, **98**, 2082–2090.
59 A. Sokolov, I. S. Aranson, J. O. Kessler and R. E. Goldstein, *Phys. Rev. Lett.*, 2007, **98**, 158102.
60 P. E. Sheehan and L. J. Whitman, *Nano Lett.*, 2005, **5**, 803–807.
61 S. Sundararajan, P. E. Lammert, A. W. Zudans, V. H. Crespi and A. Sen, *Nano Lett.*, 2008, **8**, 1271–1276.
62 D. Kagan, R. Laocharoensuk, M. Zimmerman, C. Clawson, S. Balasubramanian, D. Kang, D. Bishop, S. Sattayasamitsathit, L. Zhang and J. Wang, *Small*, 2010, **6**, 2741–2747.
63 L. Baraban, D. Makarov, R. Streubel, I. Monch, D. Grimm, S. Sanchez and O. G. Schmidt, *ACS Nano*, 2012, **6**, 3383–3389.
64 G. Zhao and M. Pumera, *Nanoscale*, 2014, **6**, 11177–11180.